

The *Hubble* Missing Globular Cluster Survey

I. Survey overview and the first precise age estimate for ESO452-11 and 2MASS-GC01

D. Massari¹, M. Bellazzini¹, M. Libralato², A. Bellini³, E. Dalessandro¹, E. Ceccarelli^{1,4}, F. Aguado-Agelet^{5,6}, S. Cassisi^{7,8}, C. Gallart^{6,9}, M. Monelli^{6,9,10}, A. Mucciarelli^{4,1}, E. Pancino¹¹, M. Salaris^{12,7}, S. Saracino^{11,12}, E. Dodd¹³, F. R. Ferraro⁴, E. R. Garro¹⁴, B. Lanzoni⁴, R. Pascale¹, and L. Rosignoli^{4,1}

¹ INAF - Astrophysics and Space Science Observatory of Bologna, Via Gobetti 93/3, 40129 Bologna, Italy
e-mail: davide.massari@inaf.it

² INAF, Osservatorio Astronomico di Padova, Vicolo dell'Osservatorio 5, Padova, I-35122, Italy

³ Space Telescope Science Institute, 3700 San Martin Drive, Baltimore, MD 21218, USA

⁴ Department of Physics and Astronomy, University of Bologna, Via Gobetti 93/2, 40129 Bologna, Italy

⁵atlanTTic, Universidade de Vigo, Escola de Enxeñaría de Telecomunicación, 36310, Vigo, Spain

⁶ Universidad de La Laguna, Avda. Astrofísico Fco. Sánchez, E-38205 La Laguna, Tenerife, Spain

⁷ INAF - Osservatorio Astronomico di Abruzzo, Via M. Maggini, 64100 Teramo, Italy

⁸ INFN - Sezione di Pisa, Università di Pisa, Largo Pontecorvo 3, 56127 Pisa, Italy

⁹ Instituto de Astrofísica de Canarias, Calle Vía Láctea s/n, E-38206 La Laguna, Tenerife, Spain

¹⁰ INAF - Osservatorio Astronomico di Roma, Via Frascati 33, 00078 Monte Porzio Catone, Roma, Italy

¹¹ INAF - Osservatorio Astrofisico di Arcetri, Largo E. Fermi 5, I-50125 Firenze, Italy

¹² Astrophysics Research Institute, Liverpool John Moores University, 146 Brownlow Hill, Liverpool L3 5RF, UK

¹³ Institute for Computational Cosmology & Centre for Extragalactic Astronomy, Department of Physics, Durham University, South Road, Durham, DH1 3LE, UK

¹⁴ ESO - European Southern Observatory, Alonso de Cordova 3107, Vitacura, Santiago, Chile

Received XX; accepted YY

ABSTRACT

We present the *Hubble* Missing Globular Cluster Survey (MGCS), a *Hubble Space Telescope* treasury programme dedicated to the observation of all the kinematically confirmed Milky Way globular clusters that missed previous *Hubble* imaging. After introducing the aims of the programme and describing its target clusters, we showcase the first results of the survey. These are related to two clusters, one located at the edge of the Milky Way Bulge and observed in optical bands, namely ESO452-11, and one located in the Galactic Disc observed in the near-IR, namely 2MASS-GC01. For both clusters, the deep colour-magnitude diagrams obtained from the MGCS observations reach several magnitudes below their main-sequence turn-off, and thus enable the first precise estimate of their age. By using the methods developed within the CARMA project, we find ESO452-11 to be an old, metal-intermediate globular cluster, with $[M/H] \approx -0.80_{-0.11}^{+0.08}$ and an age of $t = 13.59_{-0.69}^{+0.48}$ Gyr. Its location on the age-metallicity relation makes it consistent with an in-situ origin, in agreement with its dynamical properties. On the other hand, the results for 2MASS-GC01 highlight it as a young, metal-intermediate cluster, with an age of $t = 7.22_{-1.11}^{+0.93}$ Gyr at $[M/H] = -0.73_{-0.06}^{+0.06}$. This is the first ever age estimate for this extremely extincted cluster, and indicates it either as the youngest globular known to date, or as a massive and compact open cluster, which is consistent with its almost circular, disc-like orbit.

Key words. Galaxy: structure – globular clusters: general – techniques: photometric – Stars: imaging

1. Introduction

Globular clusters (GCs) are among the most powerful tracers of the early history of the Milky Way (MW). Investigating the *system* of MW GCs with the aim of reconstructing the formation and the assembly of the Galactic halo dates back to the seminal works by Kinman (1959) and Searle & Zinn (1978). Since then, many works have combined the information on intrinsic properties of GCs like age (see e.g., Marín-Franch et al. 2009, Forbes & Bridges 2010, Leaman et al. 2013, Kruijssen et al. 2019, Massari et al. 2023) or chemistry (e.g., Fall & Rees 1985, Recio-Blanco 2018, Horta et al. 2020, Monty et al. 2023, Ceccarelli et al. 2024a) to understand the origin of individual GCs, e.g., if they were born *in-situ* or accreted during past merger events.

With the systematic availability of dynamical information on the GC orbits, achieved thanks to the advent of the *Gaia* mission (Gaia Collaboration et al. 2016), this effort made huge steps forward. The addition of this information has in fact led to a rather robust classification of *in-situ* and accreted GCs (Massari et al. 2019, Forbes 2020, Callingham et al. 2022, Malhan et al. 2022, Belokurov & Kravtsov 2024, Chen & Gnedin 2024), and to the first attempts in identifying the different galaxy progenitors of the accreted ones.

The next step forward in investigating MW GCs as tracers of the Galactic evolution is improving the *accuracy* on the measurement of their properties. From the kinematic point of view, this has already been achieved thanks to the homogeneous measurement, by the same instrument (the ESA-*Gaia* mission, see, e.g.,

Gaia Collaboration et al. 2016, 2023, and references therein), of the cluster positions and proper motions (see e.g., Vasiliev & Baumgardt 2021). The measurement of the GC distance still suffers for inhomogeneity in the adopted methods, though attempts to overcome the related systematic errors has led to typical accuracies of a few per cent (Baumgardt & Vasiliev 2021). From the chemical point of view, things are more complex. The sources of systematic offsets among different abundance measurements are many, and range from the instrumental setups (wavelength range, spectral resolution, etc.), to the assumptions on the atmospheric models and the atomic parameters, to the methods used to estimate the atmospheric parameters and the elemental abundances. Also in this case, increasing effort is being dedicated to improve the abundance homogeneity among different sources (see e.g., Thomas et al. 2024), but offsets as large as a few 0.1 dex are still common, at least for some element (e.g., Carretta & Bragaglia 2023, Schiavon et al. 2024).

Concerning age measurements, and more in general any photometric study, one single facility has historically revolutionized our knowledge on GCs: the *Hubble Space Telescope* (HST). Its exquisite spatial resolution, coupled to the high sensitivity in passbands ranging from the ultra-violet (UV) to the near-infrared (NIR), has paved the way to a monumental advance in a plethora of GC-related science cases. These range from the investigation of the GC multiple populations (e.g., Milone et al. 2012), to the study of their ages (Marín-Franch et al. 2009, Dotter et al. 2010), mass function (e.g., Paust et al. 2010), and binary fraction (e.g., Milone et al. 2012), and to the characterisation of their hottest stars like white dwarfs (e.g. Bedin et al. 2023), blue/extreme horizontal branch stars (e.g. Brown et al. 2016) and blue stragglers (e.g. Ferraro et al. 2012). Some of these achievements were obtained by means of many focused GO HST programs, but the advent of large observational campaigns such as the ACS Survey of Galactic Globular Clusters (Sarajedini et al. 2007), or the HST UV Legacy Survey of Galactic Globular Clusters (Piotto et al. 2015), have effectively shaped the state-of-the-art of GC science, and after more than 10 years from their completion these data still have a huge value for the community. In spite of the monumental scientific return of existing HST observations, the heritage of HST for Galactic GCs is still significantly incomplete. In light of the most recent discoveries of new Milky Way GCs, there are still 33 kinematically confirmed GCs, either via proper motions (Vasiliev & Baumgardt 2021), or via radial velocities (see Baumgardt & Vasiliev 2021, Pace et al. 2023, Garro et al. 2023), that lack any kind of HST imaging, plus one that only has observations in one passband.

The Missing Globular Cluster Survey (MGCS, HST Treasury Program GO-17435, PI: Massari) targets these 34 GCs with the aim of providing homogeneous two-bands photometry and astrometry for each of them. The survey has three main Key objectives:

1. *Age determination.* The main goal of the *Hubble* MGCS is the determination of the age of the targets. With the precision enabled by the HST imaging and the methods developed by the Clusters Age to Reconstruct the Milky way Assembly (CARMA) collaboration (< 500 Myr on relative ages, VandenBerg et al. 2013, Massari et al. 2023), MGCS will estimate the age of the 34 clusters sampling for the first time several magnitudes below their MSTO. The age estimates will be used in combination with metallicity measurements and with the clusters orbital properties derived from *Gaia* data, to robustly assess their former galaxy progenitor (see e.g., Massari et al. 2019, Callingham et al. 2022), and to derive fundamental properties of the merger events that have led them into the Milky Way, such as the merger mass and accretion time (Kruijssen et al. 2019).
2. *Search for Bulge fossil relics.* Deep and high-resolution imaging of star clusters in the Galactic bulge has revealed the existence of a class of systems, called “bulge fossil fragments”, that might be important contributors to the build-up of the MW Bulge (Ferraro et al. 2021). These systems are all characterised by very complex color-magnitude diagrams (CMDs) indicating the coexistence of multi-age and multi-metallicity sub-populations, such as in the case of Terzan 5 (Ferraro et al. 2009, 2016, Origlia et al. 2011, 2013, Massari et al. 2014) and Liller 1 (Ferraro et al. 2021, Dalessandro et al. 2022, Crociati et al. 2023, Alvarez Garay et al. 2024, Fanelli et al. 2024). The MGCS targets a large number of still unexplored Bulge GC-like systems, and will explore their photometric properties in search for evidence of complex internal evolution, which might reveal a similar nature to that of Terzan 5 and Liller 1.
3. *Mass function.* The distribution of the individual masses of stars at their birth defines the so-called initial mass function (IMF). Whether the IMF is universal for all GCs or not has long been debated (Bastian et al. 2010), but recent investigations seem to point out that it might depend on the environment in which each cluster was born (Hénault-Brunet et al. 2019, Cadelano et al. 2020). The IMF is therefore a potential tracer of the origin of a GC. The IMF can be derived from the present-day mass function (PDMF), which differs from the IMF because GCs preferentially lose low-mass stars during their dynamical evolution (e.g., De Marchi et al. 2010). The simultaneous measurement of the global PDMF and its radial variation makes it possible to reconstruct (Webb et al. 2017, Cadelano et al. 2020) the information on the clusters IMF in relative terms (i.e., recognising GCs sharing the same IMF). The MGCS samples the targets spatial extent typically out to ~ 2 half-light radii (r_h), and the simultaneous request for parallel fields in the same bands and with similar depth will enable measuring the clusters PDMF and its radial variation out to $\sim 6 - 7 r_h$, thus to recognize GCs having the same IMF. By coupling this information with the GC orbital properties the MGCS aims at identifying cluster siblings born in the same progenitor galaxy with a completely novel approach. Furthermore, accurate and deep PDMF measurements also enable estimating the GC mass and mass-to-light ratio (Baumgardt et al. 2020), which are poorly constrained for most of the MGCS targets.

The key objectives listed above are prime examples of a plethora of other science cases of high interest for the community that the MGCS will enable investigating. Among the most remarkable, we mention here: *i*) the study of photometric binaries, and the dependence of the binary fraction on the different environment of origin (Sollima et al. 2022); *ii*) the study of Blue Stragglers as probes of the dynamical processes governing a GC evolution (Ferraro et al. 2012); *iii*) the derivation of new constraints on the structural parameters of the clusters, in particular for the surface density profile of their innermost regions; *iv*) the photometric investigation of chemical peculiarities in GC stellar populations in terms of [Fe/H], He and C+N+O abundances in the optical CMDs (detected as multiple evolutionary sequences, see e.g. Bellini et al. 2013); *v*) the improvement of the absolute proper motion determination for each target, that will be achieved by pairing the MGCS observations with first-epoch *Gaia* measurements (e.g. Massari et al. 2017, 2018, del

Pino et al. 2022); *vi*) finally, these observations will provide invaluable first epoch measurements for any future proper motion study, even in combination with other high-resolution cameras (Massari et al. 2020, Häberle et al. 2021, Libralato et al. 2022, 2023) that will provide large temporal baselines in the future.

This first paper of the MGCS series is organised as follows. In Sect. 2 we present the clusters targeted by the survey, and provide the key information about their observations. In Sect. 3 we show the first scientific application, consisting in the age measurement of two surveyed clusters, namely ESO452-11 in the optical and 2MASS-GC01 in the NIR. Last, in Sect. 4 we discuss the results and draw the final conclusions.

2. Selection of the sample and observations

The targets of the survey have been selected from a number of catalogs, including the compilations by Harris (1996), Vasiliev & Baumgardt (2021), Baumgardt & Vasiliev (2021), Pace et al. (2023) and the online database by Holger Baumgardt¹. We excluded GC candidates missing robust kinematic confirmation, and ended up with 34 systems lacking sufficient HST observations to at least build-up a CMD. Most of these 34 systems can be divided into two broad classes (see Fig. 1). The first is that of low-surface brightness GCs located in the distant halo. The classification as GCs of a few of these, like Kaposov-1 and Kaposov-2, is still debated (Koposov et al. 2007), and will be addressed as part of the scientific objectives of the survey. These twenty-seven targets are located in regions of the sky with sufficiently low reddening that they can be observed with the Wide Field Channel of the Advanced Camera for Survey (ACS/WFC), following a strategy similar to that defined by Sarajedini et al. (2007). We will therefore refer to these targets as to the *ACS sample*. We favoured the ACS camera over the Wide Field Camera 3 (WFC3) because its field of view is $\sim 40\%$ larger and thus it is better suited to investigate the radial behavior of the GC properties. The chosen F606W and F814W bands were selected because they are perfectly suited for the primary science cases of the survey, as *i*) they minimize the effect that chemical peculiarities in light-element abundances (the multiple populations phenomenon Gratton et al. 2004, Milone & Marino 2022) have on making the GCs CMD more complex, thus increasing the precision of the estimated GCs age; *ii*) they are sensitive to internal differences in age and $[\text{Fe}/\text{H}]$, thus being efficient tools to find evidence for complex internal GC evolution (e.g., Bedin et al. 2004); *iii*) they are efficient in sampling very low-mass, faint GC stars, to explore the mass function to its widest extent (Paust et al. 2010). The details of the observations of the ACS sample are summarised in Tab. 1.

The second class consists of seven GCs hidden in the highly crowded and extinct regions of the Galactic Bulge, where reddening exceeds $E(B - V) > 2$. These clusters occupy regions of the parameter space (in terms of mass, density and evolution environment) that are rather extreme and poorly sampled by existing observations, and where there is room for significant scientific advancement. These GCs have been imaged with the IR channel of the WFC3, in the F125W and F160W bands. F125W is preferred over the wider F110W because it makes the observations more efficient due to the extreme extinction. These IR bands can cause the faint main sequence of a GC CMD to split because of the aforementioned phenomenon of multiple-populations (Milone et al. 2017), but this effect takes place well

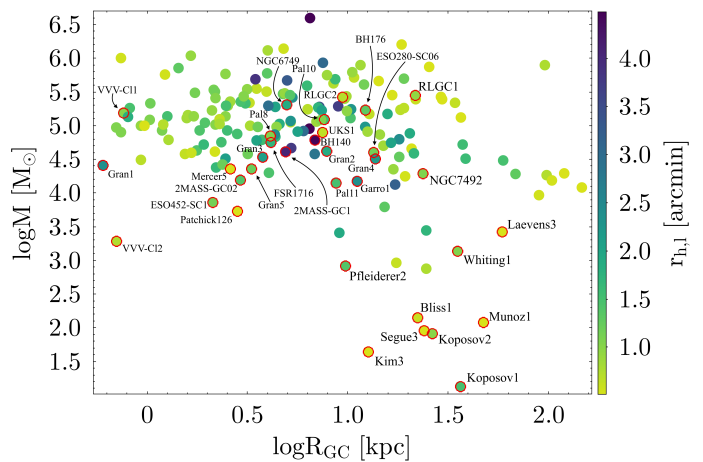


Fig. 1: Distribution of the targets of MGCS (labelled and highlighted with red circles) in the Galactocentric distance vs. mass plane. Each cluster is colour-coded according to its half-light radius.

below the MSTO point, and thus does not affect neither the age estimates, nor mass-function studies (the mass-luminosity relation along the GC main sequence is not altered significantly). The details of the observations of the WFC3/IR sample are summarised in Tab. 2.

The MGCS data reduction follows the well-established workflow outlined in various papers focused on high-precision astrometry and photometry with *HST* images (e.g., Bellini et al. 2017, Nardiello et al. 2018, Libralato et al. 2022), and it will be detailed in a forthcoming paper (Libralato et al., in prep.). Briefly, our data reduction consists in two steps called *first-pass* and *second-pass* photometry. The *first-pass* photometry measures position and flux of bright, relatively-isolated sources in each image via effective-point-spread-function (ePSF) fit. For the ACS/WFC and WFC3/UVIS analyses, we make use of the `_flc` images (which are dark and bias corrected, have been flat-fielded, pipeline-corrected for the charge-transfer-efficiency defects as described in Anderson & Ryon 2018, and are not resampled), whereas for the WFC3/IR case, `_flt` images (the analogue of the `_flc` images but without the charge-transfer-efficiency correction) are employed. The ePSF models are obtained starting from the publicly-available² library *HST* ePSFs, which are fine-tuned for each exposure. Positions are corrected for geometric distortion using the publicly-available³ *HST* corrections described in various papers (Anderson & King 2006, Bellini & Bedin 2009, Bellini et al. 2011, Anderson 2016).

These initial sets of positions and fluxes are used to set up a common reference frame system where they can be properly combined in the subsequent step. Astrometrically, such common reference-frame system is designed by means of the *Gaia* DR3 catalogue, which fixes the axis orientations (x pointing to the West and y to the North, respectively), scale (40 mas yr^{-1} and 130 mas yr^{-1} for the GCs in the optical and IR samples, respectively) and position of the clusters' center in the pixel-based frame (chosen for each target so to have only positive pixel-based coordinates). Photometrically, instrumental magnitudes are rescaled to the magnitude of the longest exposure in each camera/filter.

¹ <https://people.smp.uq.edu.au/HolgerBaumgardt/globular/orbits.html>

² <https://www.stsci.edu/~jayander/HSTIPASS/LIB/PSFs/>

³ <https://www.stsci.edu/~jayander/HSTIPASS/LIB/GDCs/STDGDCs/>

Table 1: Observing log for the ACS sample. Exposure times and filters are the same for the parallel fields observed with the WFC3/UVIS camera. Target positions are taken from (Harris 1996, 2010 edition), or from Baumgardt & Vasiliev (2021) when missing in the former catalogue.

Name	α_{2000} (h m s)	δ_{2000} ($^{\circ}$ ' ")	UT Date	Filter	Exposure Time
WHITING 1	02 02 57.0	-03 15 10.0	2024-06-19	F814W F606W	1 × 30 s, 2 × 699 s, 1 × 567 s
KOPOSOV 1	11 59 18.4	+12 15 35.8	2024-03-26 2024-05-22	F606W F814W	1 × 30 s, 2 × 699 s, 1 × 567 s 1 × 30 s, 2 × 699 s, 1 × 567 s
KOPOSOV 2	07 58 17.0	+26 15 19.4	2024-03-26 2024-05-22	F606W F814W	1 × 30 s, 2 × 699 s, 1 × 575 s 1 × 30 s, 2 × 699 s, 1 × 575 s
MUNOZ 1	15 01 48.0	+66 58 07.3			
ESO-280-6	18 09 06.0	-46 25 24.0			
Pal 8	18 41 29.9	-19 49 33.1	2024-03-16 2024-03-24	F606W F814W	1 × 30 s, 2 × 699 s, 1 × 570 s 1 × 30 s, 2 × 699 s, 1 × 570 s
Pal 11	19 45 14.4	-08 00 26.1	2024-03-14 2024-03-17	F606W F814W	1 × 30 s, 2 × 699 s, 1 × 566 s 1 × 30 s, 2 × 699 s, 1 × 566 s
Laevens 3	21 06 54.3	+14 58 48.0		F606W F814W	
NGC 7492	23 08 26.7	-15 36 41.3	2024-05-16 2024-05-12	F606W F814W	1 × 30 s, 2 × 699 s, 1 × 570 s 1 × 30 s, 2 × 699 s, 1 × 570 s
NGC 6749	19 05 15.4	+01 53 59.9	2024-03-09 2024-03-12	F606W F814W	1 × 30 s, 2 × 699 s, 1 × 337 s 1 × 30 s, 2 × 699 s, 1 × 337 s
FSR 1716	16 10 33.0	-53 44 12.0	2024-01-25 2024-02-14	F606W F814W	1 × 80 s, 2 × 699 s, 1 × 337 s 1 × 80 s, 2 × 699 s, 1 × 337 s
RLGC 1	16 17 08.4	-44 35 38.6			
Gran 2	17 11 33.6	-24 50 56.4	2024-02-06	F606W, F814W	1 × 30 s, 2 × 699 s, 1 × 570 s
Gran 3	17 05 01.4	-35 29 45.6			
Gran 4	18 32 27.1	-23 06 50.4	2024-03-17 2024-03-21	F606W F814W	1 × 30 s, 2 × 699 s, 1 × 570 s 1 × 30 s, 2 × 699 s, 1 × 570 s
Garro 1	14 09 00.0	-65 37 12.0	2024-05-22 2024-07-14	F606W F814W	1 × 40 s, 3 × 699 s
Gran 5	17 48 54.7	-24 10 12.0	2024-03-22	F606W, F814W	1 × 30 s, 2 × 699 s, 1 × 337 s
ESO-452-11	16 39 25.5	-28 23 52.1	2024-02-14 2024-01-29	F606W F814W	1 × 80 s, 2 × 699 s, 1 × 337 s 1 × 80 s, 2 × 699 s, 1 × 337 s
Gran 1	17 58 36.6	-32 01 10.8	2024-03-21	F606W, F814W	1 × 80 s, 2 × 699 s, 1 × 337 s
Pal 10	19 18 02.1	+18 34 17.9	2024-03-12 2024-03-16	F606W F814W	1 × 30 s, 2 × 699 s, 1 × 337 s 1 × 30 s, 2 × 699 s, 1 × 337 s
BH 140	12 53 00.3	-67 10 28.0	2024-04-03 2024-05-24	F606W F814W	1 × 30 s, 2 × 699 s, 1 × 337 s 1 × 30 s, 2 × 699 s, 1 × 337 s
Patchick 126	17 05 38.6	-47 20 32.0	2024-05-21 2024-01-31	F606W F814W	1 × 50 s, 2 × 699 s, 1 × 337 s 1 × 50 s, 2 × 699 s, 1 × 337 s
Bliss 1	11 50 02.6	-41 46 19.2	2025-01-08	F606W, F814W	1 × 30 s, 2 × 699 s, 1 × 647 s
Kim 3	13 22 45.2	-30 36 03.5	2024-05-19	F606W, F814W	1 × 30 s, 2 × 699 s, 1 × 590 s
Segue 3	21 21 31.0	+19 07 02.0			
PWM 2	17 58 39.0	-05 04 18.0			
BH 176	15 39 07.4	-50 03 09.8	2024-03-09	F606W, F814W	1 × 50 s, 2 × 699 s, 1 × 560 s

Notes. The MGCS clusters without an observing date have not yet been imaged by the telescope at the time of the writing of this paper.

Table 2: Observing log for the WFC3/IR sample

Name	α_{2000} (h m s)	δ_{2000} ($^{\circ}$ ' ")	UT Date	Filter	Exposure Time
UKS 1	17 54 27.2	-24 08 43.0	2024-03-26	F125W, F160W	4 × 300 s, 4 × 250 s
VVV-CL01	17 54 42.5	-24 00 53.0	2024-03-31	F125W, F160W	4 × 300 s, 4 × 250 s
RLGC-02	18 45 28.2	-05 11 33.3	2024-03-13	F125W, F160W	4 × 300 s, 4 × 250 s
2MASS-GC01	18 08 21.8	-19 49 47.0	2024-03-26	F125W, F160W	4 × 300 s, 4 × 250 s
2MASS-GC02	18 09 36.5	-20 46 44.0	2024-03-27	F125W, F160W	4 × 300 s, 4 × 250 s
VVV-CL02	17 41 6.3	-28 50 42.3	2024-03-20	F125W, F160W	4 × 300 s, 4 × 250 s
Mercer 5	18 23 19.8	-13 40 07.1	2024-03-14	F125W, F160W	4 × 300 s, 4 × 250 s

Notes. As for some clusters in Table 1, VVV-CL01 has not been observed at the time of the writing of this paper.

The *second-pass* photometry is performed with the code KS2 (Anderson in prep.; Bellini et al. 2017, Nardiello et al. 2018, Libralato et al. 2022). KS2 is designed to address the needs and overcome the criticalities related to crowded environments like GCs (by ePSF subtracting all close-by neighbour prior to the ePSF fit of a source), and to properly characterize faint stars (using all exposures at once in the detection phase).

Together with positions (registered onto the ICRS system thanks to the *Gaia* DR3 catalog; Gaia Collaboration et al. 2023) and magnitudes (calibrated onto the VEGAMag system) for all detected sources in the *HST* fields, our astro-photometric catalogs will also contain several diagnostics of the quality of the ePSF fit and the photometry, as well as a parameter that can be used to infer how well the shape of a source resembles that of the ePSF (i.e., a star). In the following, the analyses on ESO452-11 and 2MASS-GC01 are performed by considering only well-measured sources selected by means of criteria similar to those described in Libralato et al. (2022), i.e., a mix of percentile-based selections on the quality of the ePSF fit, magnitude rms and “stellarity” index, number of images used in the flux measurement, impact of the neighbour flux and local sky.

3. Showcase of scientific applications: age determination

The scientific applications in this paper focus on two GCs, one for each of the ACS and WFC3/IR samples. The former is ESO452-11 (also known as 1636-283 in Harris 1996), a cluster discovered by Lauberts et al. (1981) as part of the ESO/Uppsala survey of the ESO(B) atlas. The latter is 2MASS-GC01, an extremely extinguished stellar system serendipitously discovered by Hurt et al. (2000) from the inspection of the Two Micron All-Sky Survey (2MASS, Skrutskie et al. 2006) data.

For both systems, we showcase the quality of our MGCS observations by presenting the deepest CMDs (not corrected for differential reddening) currently available in Fig. 2. Upon applying quality selection to identify well-measured stars, these CMDs enable the most precise age determination to date for these systems. We also corrected our photometry for the effects of differential reddening with the method described in Milone

et al. (2012) before performing the isochrone fitting procedure. The resulting differential reddening maps are shown in Fig. 3 (we refer the reader to Appendix A for a direct comparison between the CMDs before and after the correction.).

3.1. Colour-magnitude diagrams

The left panel of Fig. 2 shows the CMD of the ACS field approximately centered on ESO452-11 and covering a radial range between 0.0 and $\approx 2.0'$, corresponding to $\approx 1.7 r_h$ (all structural parameters are taken from Vasiliev & Baumgardt 2021). The CMD in the middle panel is from the parallel WFC3 field, sampling a radial range between 4.5' and 7.4'. Since the tidal radius of the cluster is $r_t = 4.9'$, this CMD virtually samples only the background population and the comparison between the two panels clearly reveals the main cluster sequences. From $m_{F606W} \approx 13.5$ to $m_{F606W} \approx 19.0$ and around $m_{F606W} - m_{F814W} \approx 1.2$, we can note a steep, sparsely populated Red Giant Branch (RGB), with a clumpy red Horizontal Branch (HB) at $m_{F606W} \approx 16.3$. The Sub Giant Branch (SGB) is clearly visible, bending from the base of the RGB to the Turn Off (TO) point at $m_{F606W} \approx 20.0$. Below the TO, a thin Main Sequence (MS) is clearly distinguishable down to $m_{F606W} \approx 24.5$, where it begins to be overwhelmed by the contamination from the Galactic background. The hint of a parallel sequence of cluster binary stars, to the red of the MS, can be perceived in the same magnitude range. The fact that the density along the MS is observed to decrease significantly, with respect to the TO region, already around $m_{F606W} \approx 22.0$, that is where the completeness should still be very high (e.g., Milone et al. 2012), suggests that the low mass population of cluster stars has been strongly depleted by internal relaxation and the cluster may be in the last phases of its dynamical evolution before disruption (Paust et al. 2010). Indeed, in the Baumgardt’s catalogue of GC structural parameters, the reported remaining lifetime (T_{dis}) for ESO452-11 is just $T_{dis}=0.1$ Gyr.

In the right panel of Fig. 2 it is displayed the CMD of the stars in the WFC3/IR field centered on 2MASS-GC01. The field samples the cluster out to $\approx 1.6'$ from the cluster center, that is approximately $1 r_h$ according to Bonatto & Bica (2008) and Harris (1996), but $\approx 0.4 r_h$ according to Baumgardt’s catalogue.

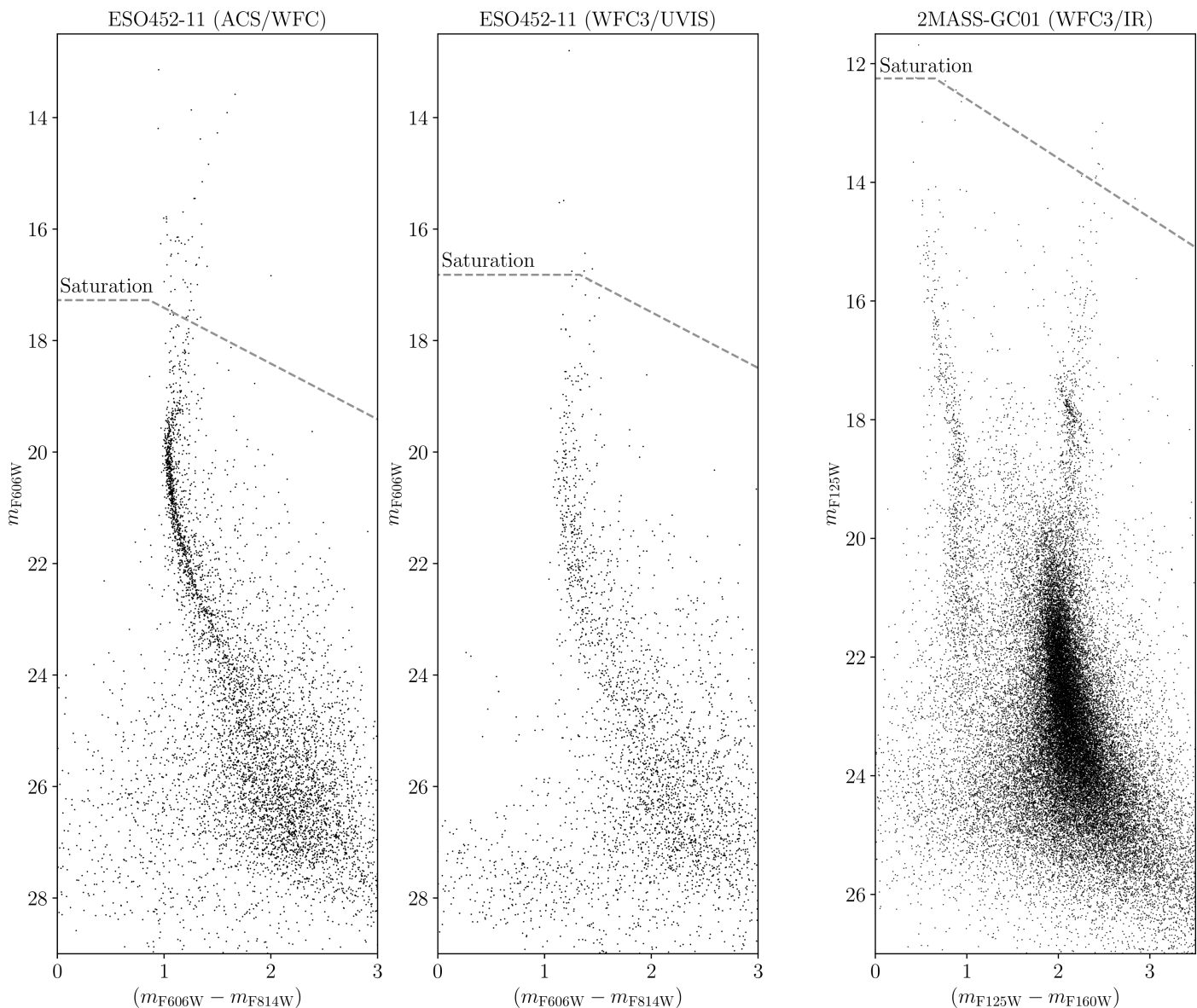


Fig. 2: Overview CMDs (not corrected for differential reddening) for ESO452-11 and 2MASS-GC01. The left and middle panels present the CMDs of ESO452-11 considering all stars in the central ACS/WFC and parallel WFC3/UVIS fields, respectively. The rightmost panel refers to the CMD of 2MASS-GC01 based on WFC3/IR data. The gray, dashed lines mark the saturation threshold.

In any case, our data sample less than half of the cluster light, around the cluster center. The extended and nearly vertical sequence that is clearly evident in the CMD for $m_{F125W} - m_{F160W} \lesssim 1.3$ is composed of local disc stars ($D \sim 1$ kpc, according to the Gaia DR3 parallaxes of its brightest members). The much redder colour of all the cluster sequences implies a significant increase of the extinction along the line of sight from the location of these stars to that of the cluster ($D \approx 3$ kpc). The RGB of the cluster is clearly seen around $m_{F125W} - m_{F160W} \approx 2.2$, running from $m_{F125W} \approx 14.0$ to $m_{F125W} \approx 21.0$, with a red HB / red clump (RC) at $m_{F125W} \approx 18.0$. The cluster upper MS is by far the most prominent feature of the entire CMD, between $m_{F125W} \approx 21.0$ and $m_{F125W} \approx 26.0$. A prominent blue plume seems to emerge from the old MS, in the colour range $1.3 \lesssim m_{F125W} - m_{F160W} \lesssim 1.8$. Further investigation is required to establish if it is a pure sequence of blue stragglers or if there is also a (largely sub-dominant) young population as found, e.g., in Liller 1 (Dalessandro et al. 2022). All the cluster sequences

are significantly elongated by the effect of differential reddening (see Fig.3, right panel).

3.2. Age estimate

The MGCS takes advantage of the methods and procedures developed within the CARMA project (Massari et al. 2023), which aims at determining the age of the entire sample of Galactic GCs in the most homogeneous way. In this sense, the MGCS perfectly fits the aims of CARMA, as the *HST* photometry is obtained in the same reference photometric system selected by CARMA, which is the one defined by the ACS filters. As a brief summary of the CARMA methods, we recall that our age determination follows an isochrone fitting approach that provides the best-fit values for age, metallicity, distance and colour-excess within a Bayesian statistical framework, thus associating robust uncertainties to all of the output parameters. In particular, the fitting procedure starts from defining the mean-ridge line of the

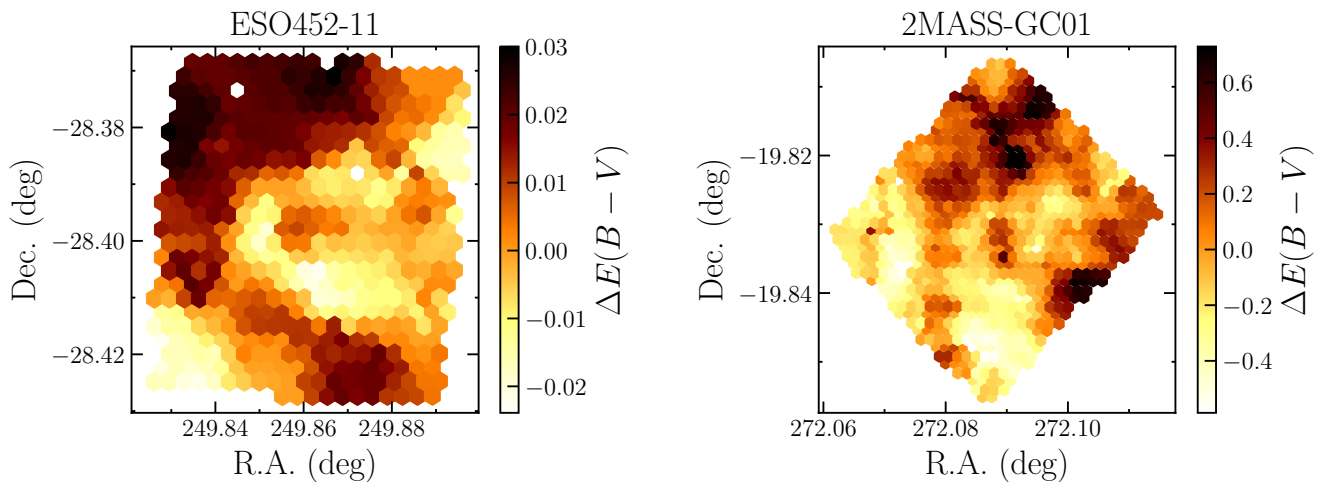


Fig. 3: Differential reddening maps for ESO452-11 (left-hand panel) and 2MASS-GC01 (right-hand panel). Please note the very different amplitude of the $\Delta E(B - V)$ scale in the two panels.

differential-reddening corrected CMD, and uses it to select the sample of stars to fit. The selection includes all stars within a certain colour range from the ridge line (see the green symbols in Fig. 4 and Fig. 5), and is applied to exclude obvious field stellar contaminants and photometric binaries, whenever the photometric quality allows it. A fine grid of solar-scaled theoretical models from the BaSTI stellar evolution library (Hidalgo et al. 2018, Pietrinferni et al. 2021) is then fit to the data via Markov Chain Monte Carlo (MCMC) sampling, starting from some loose priors on metallicity, distance and $E(B - V)$. The choice of solar-scaled models has been made to avoid making any assumptions on the α -element abundance of GCs. The term on the α -element mixture is then effectively absorbed by working in global metallicity $[M/H]$. This is justified by the fact that the MGCS photometry is in optical and NIR bands, for which the equivalency between solar-scaled and α -enhanced models at the same global metallicity has been demonstrated by Salaris et al. (1993), Cassisi et al. (2004) through the relation: $[M/H] = [Fe/H] + \log(0.694 \times 10^{[\alpha/Fe]} + 0.301)$. Finally, the median values of the resulting posterior distribution functions are used as the best-fit solution, and the 16th and 84th percentiles are taken as the asymmetric uncertainties. All the details of the method can be found in Massari et al. (2023).

Here we show the results of the age determination for the pair of GCs analysed in this work, starting with ESO452-11. From the photometric point of view, shallow, ground-based, optical and NIR observations of this cluster have suggested (Minniti et al. 1995, Bica et al. 1999, Cornish et al. 2006, Bonatto & Bica 2008) ESO452-11 is 10–16 Gyr old, with a reddening of $E(B - V) = 0.5$ –0.8 mag, a distance of 5.8–7.5 kpc and a photometric metallicity $-1.3 < [Fe/H] < -0.4$. Recent spectroscopic investigations (Koch et al. 2017, Simpson et al. 2017) determined a more precise mean metallicity of $[Fe/H] = -0.88 \pm 0.03$, with a possible spread in light elements (Simpson et al. 2017) and a slight under-abundance of the α -elements compared to the surrounding Bulge stars (Koch et al. 2017). This latter chemical feature might suggest a different origin for ESO452-11 with respect to in-situ stars. Determining a precise age and comparing that with the age of other in-situ GCs of similar metallicity will provide independent insight on the origin of ESO452-11.

Figure 4 shows the results of the fit in the $(m_{F606W} - m_{F814W}, m_{F606W})$ and $(m_{F606W} - m_{F814W}, m_{F814W})$ planes, independently. The CMDs and the best-fit isochrones are shown in the upper row, while the marginalized two and one dimensional distributions of the model parameters are shown in the bottom row. The two solutions are mutually consistent in all the parameters of the fit. As the final results, we use the average values of the two solutions, while the overall uncertainties are computed such to encompass the upper and lower limits of both runs combined. The mean colour excess is $E(B - V) = 0.54 \pm 0.01$, consistent with the previous estimates. The mean distance modulus is $(m - M)_0 = 14.29 \pm 0.03$, corresponding to a heliocentric distance of 7.2 kpc, in good agreement with (Baumgardt & Vasiliev 2021) and consistent with Cornish et al. (2006). Note, however, that adopting the integrated apparent V magnitude $V_T = 11.77 \pm 0.09$ from Baumgardt et al. (2020) and our estimates of the distance modulus and reddening, the absolute magnitudes of the cluster brightens from $M_V = -3.82$, as reported in Baumgardt et al. (2020), to $M_V = -4.19 \pm 0.10$. The mean global metallicity is $[M/H] = -0.80^{+0.08}_{-0.11}$. Before comparing this to spectroscopic values, it is fundamental to convert $[M/H]$ to $[Fe/H]$, correcting by the contribution of α elements (Salaris et al. 2002). Using Eq. 3 in Salaris et al. (1993), adjusted by the different reference solar mixture of the BaSTI models (see e.g., Massari et al. 2023), and adopting the mean $[(Si + Ca + Ti)/Fe] = 0.20$ found for this cluster by Koch et al. (2017), our solution translates to $[Fe/H] = -0.94$. This is significantly different from the value of $[Fe/H] = -1.50$ quoted in Harris (1996), but consistent within 1σ with the two most recent spectroscopic investigations available in the literature (Koch et al. 2017, Simpson et al. 2017). The mean age of ESO452-11 is $t = 13.59^{+0.48}_{-0.69}$ Gyr. Given the systematic errors on the absolute age values introduced by different assumptions on the input physics of theoretical models (e.g., Chaboyer 1995), we are mainly interested in the relative age of this GC, compared to age values obtained in a strictly homogeneous way, like the ones provided by CARMA. In this sense, the cluster is older than the in-situ GCs at $[M/H] \approx -0.5$ studied in Massari et al. (2023), and it is as old as the in-situ GC NGC 288 at metallicity of $[M/H] = -1.11$ studied by Aguado-Agelet et al. (submitted), for which the authors found $t = 13.75^{+0.28}_{-0.22}$ Gyr. Therefore, these results point towards an in-situ origin for

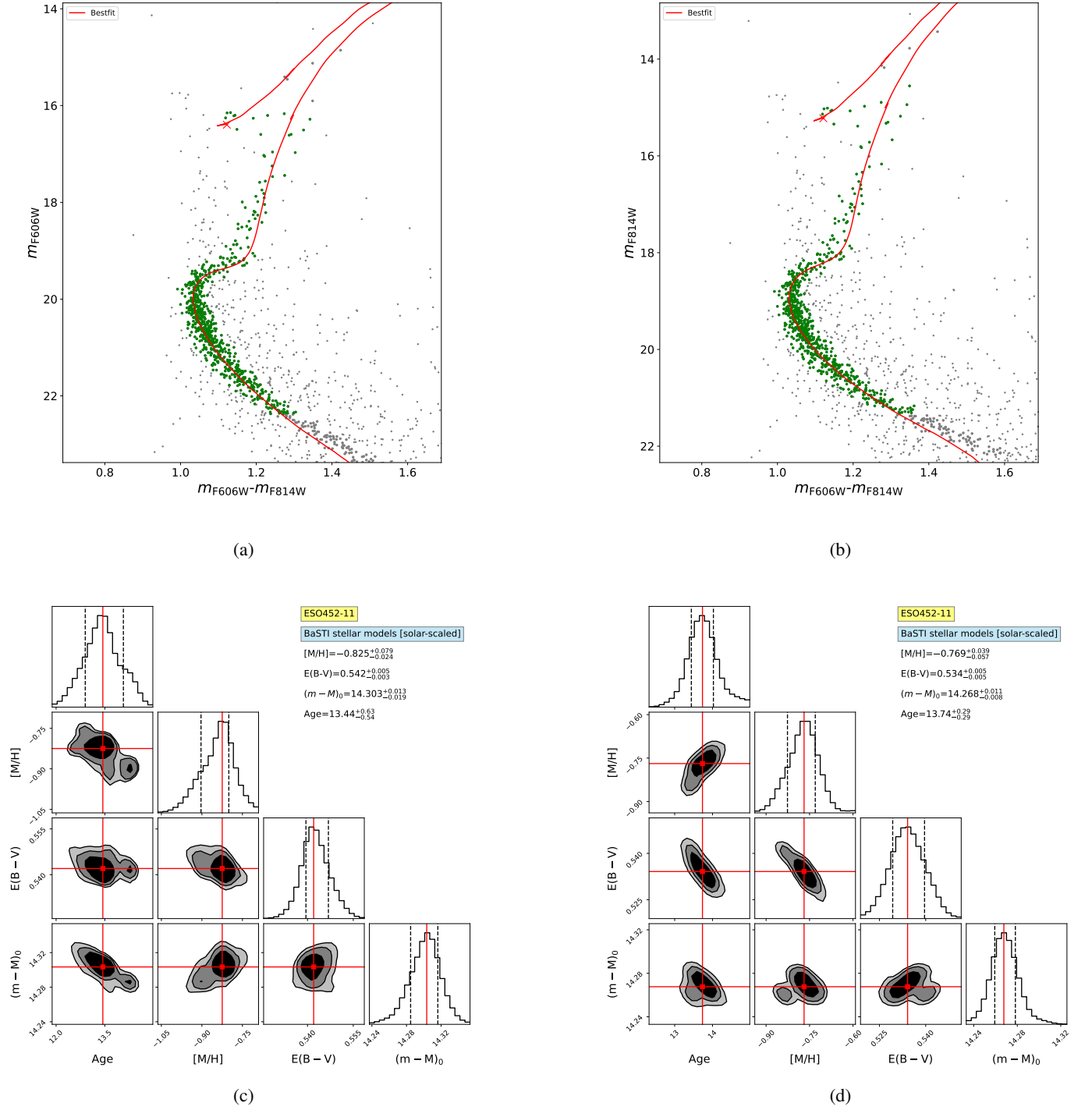


Fig. 4: Results of the isochrone fitting for ESO452-11. Panels a) and b) show the $(m_{F606W} - m_{F814W}, m_{F606W})$ and the $(m_{F606W} - m_{F814W}, m_{F814W})$ CMDs, respectively. Gray symbols describe the whole sample of stars in the cluster catalogue, while green symbols show the stars effectively used for the isochrone fit, selected as described in the text. The red line corresponds to the best-fit model. Panels c) and d) show the corresponding corner plots of the MCMC sampling.

ESO452-11, and support the classification as a bulge GC based on its orbital properties proposed by [Massari et al. \(2019\)](#) and [Callingham et al. \(2022\)](#).

The second cluster presented here, 2MASS-GC01, is a rather faint system ($M_V = -5.8$, [Bonatto & Bica 2008](#)) hidden behind thick dust clouds in the Disc. For this reason, the cluster has

been very poorly investigated prior to this work. The only information available comes from [Ivanov & Borissova \(2002\)](#), who determined a photometric metallicity of $[Fe/H] = -1.19 \pm 0.38$ and an extinction $E(B-V) \sim 6.8 \pm 0.71$. Our photometry is by far the deepest ever obtained for 2MASS-GC01, sampling ~ 2 mag below the cluster MSTO, whereas previous photom-

etry could only detect the cluster RGB. This enables a unique opportunity to estimate the age of the cluster on solid ground. As evident from the shape of the red clump in the CMD of Fig. 5, despite the differential reddening correction, the photometry still suffers from severe residual differential reddening. The age estimate is therefore more uncertain than in the case of ESO452-11, but our code still converges to reasonable solutions for the $(m_{F125W} - m_{F160W}, m_{F125W})$ and $(m_{F125W} - m_{F160W}, m_{F160W})$ CMDs, with the isochrone fit capable of well reproducing the most evident features.

In terms of average values, our combined solution points to a metallicity of $[M/H] = -0.73_{-0.06}^{+0.06}$. Since no spectroscopic measurements of the α -element abundance exist for this cluster, but its global metallicity is similar to the one found for ESO452-11, and both clusters are likely born in-situ, we assumed the same $[\alpha/Fe]$ ratio⁴, thus obtaining $[Fe/H] = -0.85_{-0.06}^{+0.07}$. This value is consistent within 1σ with the photometric metallicity derived by Ivanov & Borissova (2002). The average colour-excess and distance modulus are $E(B - V) = 7.27_{-0.03}^{+0.02}$ and $(m - M)_0 = 12.36_{-0.02}^{+0.03}$. These values are also in agreement within the (rather large) uncertainty of previous literature estimates, and make 2MASS-GC01 the most extincted cluster known in the Milky Way, located at a distance of $D = 2.96 \pm 0.04$ kpc from us, consistent with $D = 3.37 \pm 0.62$ kpc from (Baumgardt & Vasiliev 2021). However, we find a mean reddening significantly larger than what found in the literature. Assuming $V_T = 27.7$ from Baumgardt's catalogue, this leads to a much brighter absolute magnitude $M_V = -7.20 \pm 0.50$ (by arbitrarily adopting an uncertainty of 0.5 mag on V_T , since it is not reported in the catalogue).

In terms of relative age, when compared to the other Milky Way GCs for which age has been estimated in the same homogeneous way, with an average of $t = 7.22_{-1.11}^{+0.93}$ Gyr 2MASS-GC01 is very young. For reference, ESO452-11, for which we find a similar metallicity, is ~ 6.5 Gyr older. The in-situ GCs analysed in Massari et al. (2023) are also older by about more than 5 Gyr. As shown by Marín-Franch et al. (2009), a younger age at this metallicity could be indicative of an accreted origin. Within the CARMA collaboration, Aguado-Agelet et al. (submitted) estimated the age of GCs associated to the Gaia-Sausage-Enceladus merger event (Helmi et al. 2018, Belokurov et al. 2018), finding that, at $[Fe/H] \approx -1$, these GCs are younger than their in-situ counterpart by 1.5–2 Gyr, but not nearly as young as 2MASS-GC01. The location of 2MASS-GC01 on the age-metallicity plane is instead more consistent with that described by Milky Way Disk stars during a late, quiescent phase of star formation, as found by Xiang & Rix (2022). Incidentally, these authors found such a late phase to start at an age of about 8 Gyr, which is similar to the age we estimated for 2MASS-GC01 (but we remark once again that these absolute values should be compared with great caution).

3.3. The nature of 2MASS-GC01

The findings presented here could be interpreted as evidence for 2MASS-GC01 to be an open cluster (OC) rather than a GC. On the one hand, this conclusion is fully consistent with the dynamical properties of the cluster. In fact, by integrating its orbit in the MW gravitational potential of McMillan (2017), with the prescriptions listed in Massari et al. (2019) and Ceccarelli et al. (2024b), and by assuming the distance determined here and the

⁴ An uncertainty of ± 0.15 on $[\alpha/Fe]$ translates to an additional uncertainty of ± 0.11 in $[Fe/H]$.

remaining five parameters of the phase space as in Baumgardt & Vasiliev (2021), we find that 2MASS-GC01 moves on a very circular, disc-like orbit. Its circularity is 0.98, with a maximum height from the Galactic plane of only $z_{max} = 0.11$ kpc and an eccentricity of 0.14 (resulting from an orbital pericentre of 4.19 kpc and an apocentre of 5.56 kpc), this strongly suggesting an in-situ origin in the Galactic thin disc.

On the other hand, though, its structural parameters are not consistent with those of other typical Galactic OCs. For example, its core radius is of $r_c = 0.18$ pc (Baumgardt & Hilker 2018), which is below the lower limit of the OC distribution studied in Tarricq et al. (2022). Along the same line, its half-light radius is the smallest among the old OCs investigated in Alvarez-Baena et al. (2024). Its estimated mass of $4.1 \times 10^4 M_\odot$ (Baumgardt & Hilker 2018) is at the very high-mass end of the mass distribution of Galactic OCs (Cordoni et al. 2023, Just et al. 2023, Hunt & Reffert 2024), and it is even more extreme if we re-determine it by using the same mass-to-light ratio as in Baumgardt & Hilker (2018) and the absolute magnitude derived here, which increases the mass estimate to $1.1 \times 10^5 M_\odot$. Ultimately, it should be noted that the metallicity of 2MASS-GC01 is > 0.5 dex more metal-poor than open clusters at similar Galactocentric distance, also considering only OCs older than 5 Gyr (Magrini et al. 2023, Palla et al. 2024).

In conclusion, 2MASS-GC01 either looks like a peculiarly young GC orbiting in the thin disc, or a rather extreme OC in terms of mass and compactness. In the absence of a spectroscopic follow-up that can unveil the details of its chemical composition, we limit our conclusions in highlighting the possibility that the classification of 2MASS-GC01, (identified as a *candidate* GC already by Hurt et al. 2000) might have to be revisited.

4. Summary and conclusions

In this first paper of the series we have presented the *Hubble* MGCS, an imaging survey dedicated to the 34 kinematically confirmed MW GCs that lacked prior *HST* observations to build a CMD. After describing the ACS sample, consisting of 27 GCs observed in the F606W and F814W filters of the ACS/WFC, and the WFC3/IR sample, consisting of 7 GCs located in highly extincted regions of the bulge and observed through the F125W and the F160W filters of the WFC3/IR, we showcase the quality of the MGCS data on two targets. In particular, we take advantage of the deep and accurate photometry obtained from the observations of ESO452-11 and 2MASS-GC01 to provide the first precise age determination of the two clusters.

By adopting the tools and the methods developed within the CARMA project (Massari et al. 2023), we find ESO452-11 to be a $13.59_{-0.69}^{+0.48}$ Gyr old GC at an intermediate metallicity of $[M/H] = -0.80$. These values make ESO452-11 as old as the in-situ GC NGC 288 at $[M/H] \approx -1.11$ (Ceccarelli et al. subm.), and about 1 Gyr older than the in-situ GCs at $[M/H] \approx -0.5$ investigated in Massari et al. (2023). These results thus confirm the in-situ origin of this system, already suggested in previous works based on its orbital properties (e.g., Massari et al. 2019, Callingham et al. 2022).

On the other hand, the isochrone fitting procedure applied to the CMD of 2MASS-GC01 revealed a remarkably young age of $t = 7.22_{-1.11}^{+0.93}$ Gyr at a metallicity $[M/H] = -0.73$. Such an age is significantly younger than the youngest among the accreted GCs belonging to the Gaia-Sausage-Enceladus merger event (Aguado-Agelet et al. subm.), and is more consistent with the start of the late phase of quiescent star formation in the MW

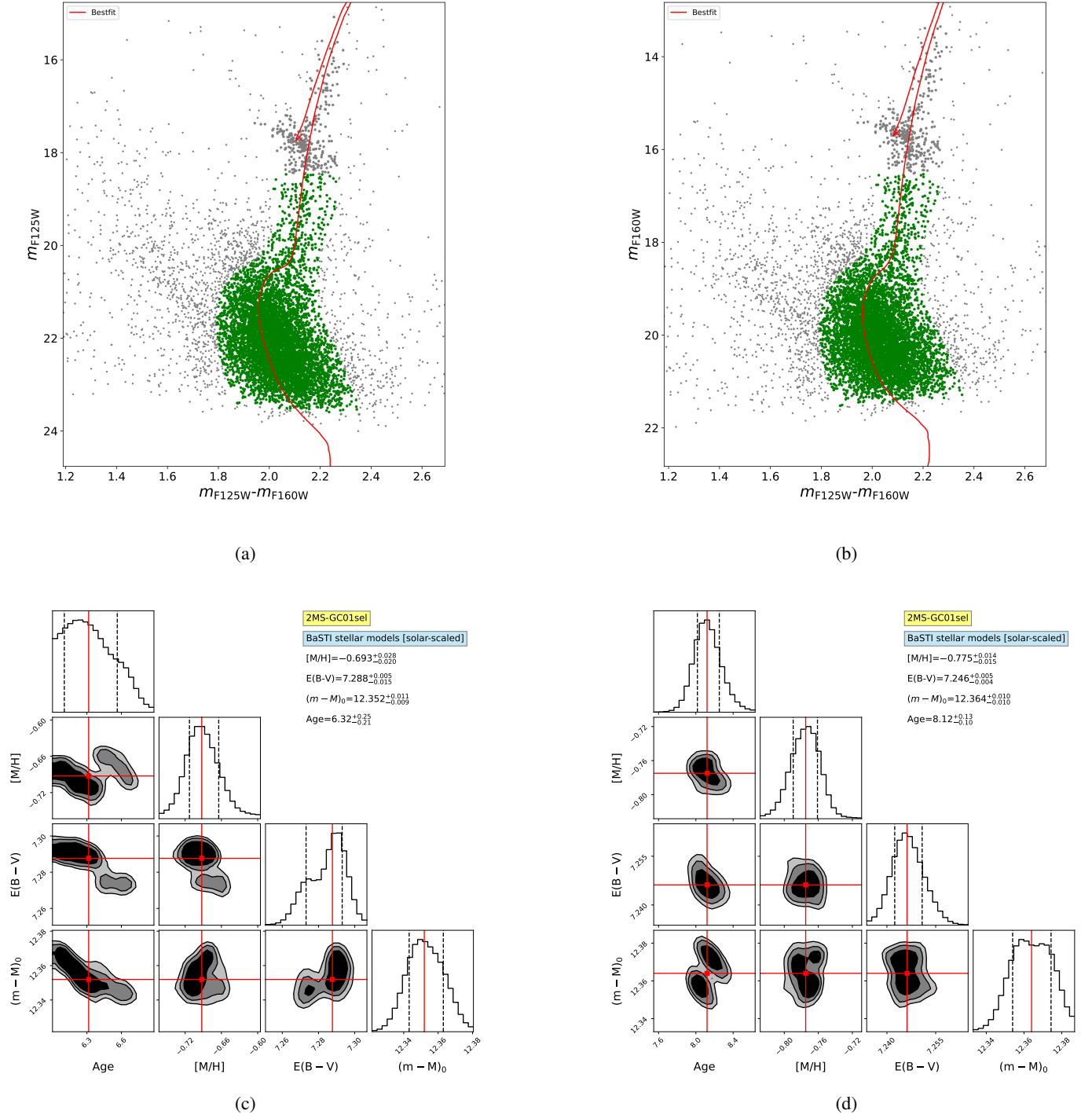


Fig. 5: Results of the isochrone fitting for 2MASS-GC01.

disc as found by [Xiang & Rix \(2022\)](#). Moreover, we computed the cluster orbit using the distance estimate derived from our isochrone fitting, and find an almost circular orbit with a very limited excursion above the Galactic plane. For these reasons, our findings suggest that 2MASS-GC01 might be a massive OC rather than a GC. However, the metallicity derived here highlights the cluster as an extreme outlier of the Galactic metallicity gradient as traced by OCs. Moreover, its structural parameters are significantly off from the typical values observed in other

OCs. Hence, we prefer to wait for an adequate and detailed spectroscopic abundance analysis before drawing firm conclusions on the nature of this system.

The simple scientific applications to the MGCS dataset shown in this paper demonstrate the power that these *HST* observations have in pushing our knowledge on GCs beyond its current limits. Calibrated and geometric-distortion corrected astrophotometric catalogues including quality parameters for an appropriate sample selection, differential reddening maps, and cat-

alogues of artificial stars for each target of the survey will be released to the public, thus completing the legacy of *HST* in this paramount field of astronomical research.

Acknowledgements. DM, SC, EP and AM acknowledge financial support from PRIN-MIUR-22: CHRONOS: adjusting the clock(s) to unveil the CHRONO-chemo-dynamical Structure of the Galaxy" (PI: S. Cassisi). SS acknowledges funding from the European Union under the grant ERC-2022-AdG, "*StarDance: the non-canonical evolution of stars in clusters*", Grant Agreement 101093572, PI: E. Pancino. A.M. and M.B. acknowledge support from the project "LEGO – Reconstructing the building blocks of the Galaxy by chemical tagging" (P.I. A. Mucciarelli), granted by the Italian MUR through contract PRIN 2022LLP8TK_001. CG acknowledges support from the Agencia Estatal de Investigación del Ministerio de Ciencia e Innovación (AEI-MCINN) under grant "At the forefront of Galactic Archaeology: evolution of the luminous and dark matter components of the Milky Way and Local Group dwarf galaxies in the Gaia era" with reference PID2020-118778GB-I00/10.13039/501100011033. CG also acknowledge support from the Severo Ochoa program through CEX2019-000920-S. TRL acknowledges support from Juan de la Cierva fellowship (JC2020-043742-I), financed by MCIN/AEI/10.13039/501100011033. M.M. acknowledges support from the Agencia Estatal de Investigación del Ministerio de Ciencia e Innovación (MCIN/AEI) under the grant "RR Lyrae stars, a lighthouse to distant galaxies and early galaxy evolution" and the European Regional Development Fun (ERDF) with reference PID2021-127042OB-I00. Co-funded by the European Union (ERC-2022-AdG, "StarDance: the non-canonical evolution of stars in clusters", Grant Agreement 101093572, PI: E. Pancino). Views and opinions expressed are however those of the author(s) only and do not necessarily reflect those of the European Union or the European Research Council. Neither the European Union nor the granting authority can be held responsible for them. This paper is supported by the Italian Research Center on High Performance Computing Big Data and Quantum Computing (ICSC), project funded by European Union - NextGenerationEU - and National Recovery and Resilience Plan (NRRP) - Mission 4 Component 2 within the activities of Spoke 3 (Astrophysics and Cosmos Observations). This work is part of the project Cosmic-Lab at the Physics and Astronomy Department "A. Righi" of the Bologna University (<http://www.cosmic-lab.eu/Cosmic-Lab/Home.html>). Based on observations with the NASA/ESA HST, obtained at the Space Telescope Science Institute, which is operated by AURA, Inc., under NASA contract NAS 5-26555. Support for Program number GO-17435 was provided through grants from STScI under NASA contract NAS5-26555. This research made use of emcee (Foreman-Mackey et al. 2013). This work has made use of data from the European Space Agency (ESA) mission *Gaia* (<https://www.cosmos.esa.int/gaia>), processed by the *Gaia* Data Processing and Analysis Consortium (DPAC, <https://www.cosmos.esa.int/web/gaia/dpac/consortium>). Funding for the DPAC has been provided by national institutions, in particular the institutions participating in the *Gaia* Multilateral Agreement. This project has received funding from the European Research Council (ERC) under the European Union's Horizon 2020 research and innovation programme (grant agreement No. 804240) for S.S. and Á.S. M.M. acknowledges support from the Agencia Estatal de Investigación del Ministerio de Ciencia e Innovación (MCIN/AEI) under the grant "RR Lyrae stars, a lighthouse to distant galaxies and early galaxy evolution" and the European Regional Development Fun (ERDF) with reference PID2021-127042OB-I00, and from the Spanish Ministry of Science and Innovation (MICINN) through the Spanish State Research Agency, under Severo Ochoa Programme 2020-2023 (CEX2019-000920-S). P.J. acknowledges support from the Swiss National Science Foundation.

References

Alvarez-Baena, N., Carrera, R., Thompson, H., et al. 2024, *A&A*, 687, A101
 Alvarez Garay, D. A., Fanelli, C., Origlia, L., et al. 2024, *A&A*, 686, A198
 Anderson, J. 2016, Empirical Models for the WFC3/IR PSF, Space Telescope Science Report
 Anderson, J. & King, I. R. 2006, PSFs, Photometry, and Astronomy for the ACS/WFC, Instrument Science Report ACS 2006-01
 Anderson, J. & Ryon, J. E. 2018, Improving the Pixel-Based CTE-correction Model for ACS/WFC, Instrument Science Report ACS 2018-04, 37 pages
 Bastian, N., Covey, K. R., & Meyer, M. R. 2010, *ARA&A*, 48, 339
 Baumgardt, H. & Hilker, M. 2018, *MNRAS*, 478, 1520
 Baumgardt, H., Sollima, A., & Hilker, M. 2020, *PASA*, 37, e046
 Baumgardt, H. & Vasiliev, E. 2021, *MNRAS*, 505, 5957
 Bedin, L. R., Piotto, G., Anderson, J., et al. 2004, *ApJ*, 605, L125
 Bedin, L. R., Salaris, M., Anderson, J., et al. 2023, *MNRAS*, 518, 3722
 Bellini, A., Anderson, J., & Bedin, L. R. 2011, *PASP*, 123, 622
 Bellini, A., Anderson, J., Bedin, L. R., et al. 2017, *ApJ*, 842, 6
 Bellini, A. & Bedin, L. R. 2009, *PASP*, 121, 1419

Bellini, A., Piotto, G., Milone, A. P., et al. 2013, *ApJ*, 765, 32
 Belokurov, V., Erkal, D., Evans, N. W., Koposov, S. E., & Deason, A. J. 2018, *MNRAS*, 478, 611
 Belokurov, V. & Kravtsov, A. 2024, *MNRAS*, 528, 3198
 Bica, E., Ortolani, S., & Barbuy, B. 1999, *A&AS*, 136, 363
 Bonatto, C. & Bica, E. 2008, *A&A*, 479, 741
 Brown, T. M., Cassisi, S., D'Antona, F., et al. 2016, *ApJ*, 822, 44
 Cadelano, M., Dalessandro, E., Webb, J. J., et al. 2020, *MNRAS*, 499, 2390
 Callingham, T. M., Cautun, M., Deason, A. J., et al. 2022, *MNRAS*, 513, 4107
 Cardelli, J. A., Clayton, G. C., & Mathis, J. S. 1989, *ApJ*, 345, 245
 Carretta, E. & Bragaglia, A. 2023, *A&A*, 677, A73
 Cassisi, S., Salaris, M., Castelli, F., & Pietrinferni, A. 2004, *ApJ*, 616, 498
 Ceccarelli, E., Massari, D., Mucciarelli, A., et al. 2024a, *A&A*, 684, A37
 Ceccarelli, E., Mucciarelli, A., Massari, D., Bellazzini, M., & Matsuno, T. 2024b, *A&A*, 691, A226
 Chaboyer, B. 1995, *ApJ*, 444, L9
 Chen, Y. & Gnedin, O. Y. 2024, arXiv e-prints, arXiv:2401.17420
 Cordoni, G., Milone, A. P., Marino, A. F., et al. 2023, *A&A*, 672, A29
 Cornish, A. S. M., Phelps, R. L., Briley, M. M., & Friel, E. D. 2006, *AJ*, 131, 2543
 Crociati, C., Valenti, E., Ferraro, F. R., et al. 2023, *ApJ*, 951, 17
 Dalessandro, E., Crociati, C., Cignoni, M., et al. 2022, *ApJ*, 940, 170
 De Marchi, G., Paresce, F., & Portegies Zwart, S. 2010, *ApJ*, 718, 105
 del Pino, A., Libralato, M., van der Marel, R. P., et al. 2022, *ApJ*, 933, 76
 Dotter, A., Sarajedini, A., Anderson, J., et al. 2010, *ApJ*, 708, 698
 Fall, S. M. & Rees, M. J. 1985, *ApJ*, 298, 18
 Fanelli, C., Origlia, L., Rich, R. M., et al. 2024, *A&A*, 690, A139
 Ferraro, F. R., Dalessandro, E., Mucciarelli, A., et al. 2009, *Nature*, 462, 483
 Ferraro, F. R., Lanzoni, B., Dalessandro, E., et al. 2012, *Nature*, 492, 393
 Ferraro, F. R., Massari, D., Dalessandro, E., et al. 2016, *ApJ*, 828, 75
 Ferraro, F. R., Pallanca, C., Lanzoni, B., et al. 2021, *Nature Astronomy*, 5, 311
 Forbes, D. A. 2020, *MNRAS*, 493, 847
 Forbes, D. A. & Bridges, T. 2010, *MNRAS*, 404, 1203
 Foreman-Mackey, D., Hogg, D., Lang, D., & Goodman, J. 2013, *Publications of the Astronomical Society of the Pacific*, 125, 306
 Gaia Collaboration, Prusti, T., de Bruijne, J. H. J., et al. 2016, *A&A*, 595, A1
 Gaia Collaboration, Vallenari, A., Brown, A. G. A., et al. 2023, *A&A*, 674, A1
 Garro, E. R., Fernández-Trincado, J. G., Minniti, D., et al. 2023, *A&A*, 669, A136
 Gratton, R., Sneden, C., & Carretta, E. 2004, *ARA&A*, 42, 385
 Häberle, M., Libralato, M., Bellini, A., et al. 2021, *MNRAS*, 503, 1490
 Harris, W. E. 1996, *AJ*, 112, 1487
 Helmi, A., Babusiaux, C., Koppelman, H. H., et al. 2018, *Nature*, 563, 85
 Hénault-Brunet, V., Gieles, M., Sollima, A., et al. 2019, *MNRAS*, 483, 1400
 Hidalgo, S. L., Pietrinferni, A., Cassisi, S., et al. 2018, *ApJ*, 856, 125
 Horta, D., Schiavon, R. P., Mackereth, J. T., et al. 2020, *MNRAS*, 493, 3363
 Hunt, E. L. & Reffert, S. 2024, *A&A*, 686, A42
 Hurt, R. L., Jarrett, T. H., Kirkpatrick, J. D., et al. 2000, *AJ*, 120, 1876
 Ivanov, V. D. & Borissova, J. 2002, *A&A*, 390, 937
 Just, A., Piskunov, A. E., Klos, J. H., Kovaleva, D. A., & Polyachenko, E. V. 2023, *A&A*, 672, A187
 Kinman, T. D. 1959, *MNRAS*, 119, 538
 Koch, A., Hansen, C. J., & Kunder, A. 2017, *A&A*, 604, A41
 Koposov, S., de Jong, J. T. A., Belokurov, V., et al. 2007, *ApJ*, 669, 337
 Kruijssen, J. M. D., Pfeffer, J. L., Reina-Campos, M., Crain, R. A., & Bastian, N. 2019, *MNRAS*, 486, 3180
 Lauberts, A., Holmberg, E. B., Schuster, H. E., & West, R. M. 1981, *A&AS*, 43, 307
 Leaman, R., VandenBerg, D. A., & Mendel, J. T. 2013, *MNRAS*, 436, 122
 Libralato, M., Bellini, A., van der Marel, R. P., et al. 2023, *ApJ*, 950, 101
 Libralato, M., Bellini, A., Vesperini, E., et al. 2022, *ApJ*, 934, 150
 Magrini, L., Viscasillas Vázquez, C., Spina, L., et al. 2023, *A&A*, 669, A119
 Malhan, K., Ibata, R. A., Sharma, S., et al. 2022, *ApJ*, 926, 107
 Marin-Franch, A., Aparicio, A., Piotto, G., et al. 2009, *ApJ*, 694, 1498
 Massari, D., Aguado-Agelet, F., Monelli, M., et al. 2023, *A&A*, 680, A20
 Massari, D., Breddels, M. A., Helmi, A., et al. 2018, *Nature Astronomy*, 2, 156
 Massari, D., Helmi, A., Mucciarelli, A., et al. 2020, *A&A*, 633, A36
 Massari, D., Koppelman, H. H., & Helmi, A. 2019, *A&A*, 630, L4
 Massari, D., Mucciarelli, A., Ferraro, F. R., et al. 2014, *ApJ*, 795, 22
 Massari, D., Posti, L., Helmi, A., Fiorentino, G., & Tolstoy, E. 2017, *A&A*, 598, L9
 McMillan, P. J. 2017, *MNRAS*, 465, 76
 Milone, A. P. & Marino, A. F. 2022, *Universe*, 8, 359
 Milone, A. P., Piotto, G., Bedin, L. R., et al. 2012, *A&A*, 540, A16
 Milone, A. P., Piotto, G., Renzini, A., et al. 2017, *MNRAS*, 464, 3636
 Minniti, D., Olszewski, E. W., & Rieke, M. 1995, *AJ*, 110, 1686
 Monty, S., Yong, D., Massari, D., et al. 2023, *MNRAS*, 522, 4404
 Nardiello, D., Libralato, M., Piotto, G., et al. 2018, *MNRAS*, 481, 3382
 Origlia, L., Massari, D., Rich, R. M., et al. 2013, *ApJ*, 779, L5
 Origlia, L., Rich, R. M., Ferraro, F. R., et al. 2011, *ApJ*, 726, L20

- Pace, A. B., Koposov, S. E., Walker, M. G., et al. 2023, MNRAS, 526, 1075
- Palla, M., Magrini, L., Spitoni, E., et al. 2024, A&A, 690, A334
- Paust, N. E. Q., Reid, I. N., Piotto, G., et al. 2010, AJ, 139, 476
- Pietrinferni, A., Hidalgo, S., Cassisi, S., et al. 2021, ApJ, 908, 102
- Piotto, G., Milone, A. P., Bedin, L. R., et al. 2015, AJ, 149, 91
- Recio-Blanco, A. 2018, A&A, 620, A194
- Salaris, M., Cassisi, S., & Weiss, A. 2002, PASP, 114, 375
- Salaris, M., Chieffi, A., & Straniero, O. 1993, ApJ, 414, 580
- Sarajedini, A., Bedin, L. R., Chaboyer, B., et al. 2007, AJ, 133, 1658
- Schiavon, R. P., Phillips, S. G., Myers, N., et al. 2024, MNRAS, 528, 1393
- Searle, L. & Zinn, R. 1978, ApJ, 225, 357
- Simpson, J. D., De Silva, G., Martell, S. L., Navin, C. A., & Zucker, D. B. 2017, MNRAS, 472, 2856
- Skrutskie, M. F., Cutri, R. M., Stiening, R., et al. 2006, AJ, 131, 1163
- Sollima, A., Gratton, R., Lucatello, S., & Carretta, E. 2022, MNRAS, 512, 776
- Tarricq, Y., Soubiran, C., Casamiquela, L., et al. 2022, A&A, 659, A59
- Thomas, G. F., Battaglia, G., Gran, F., et al. 2024, arXiv e-prints, arXiv:2404.02578
- VandenBerg, D. A., Brogaard, K., Leaman, R., & Casagrande, L. 2013, ApJ, 775, 134
- Vasiliev, E. & Baumgardt, H. 2021, MNRAS, 505, 5978
- Webb, J. J., Vesperini, E., Dalessandro, E., et al. 2017, MNRAS, 471, 3845
- Xiang, M. & Rix, H.-W. 2022, Nature, 603, 599

Appendix A: Differential reddening corrected CMDs

Figure [A.1](#) shows the CMDs of the two clusters studied here, before and after the differential reddening correction. The corresponding reddening maps are shown in [Sect. 3](#).

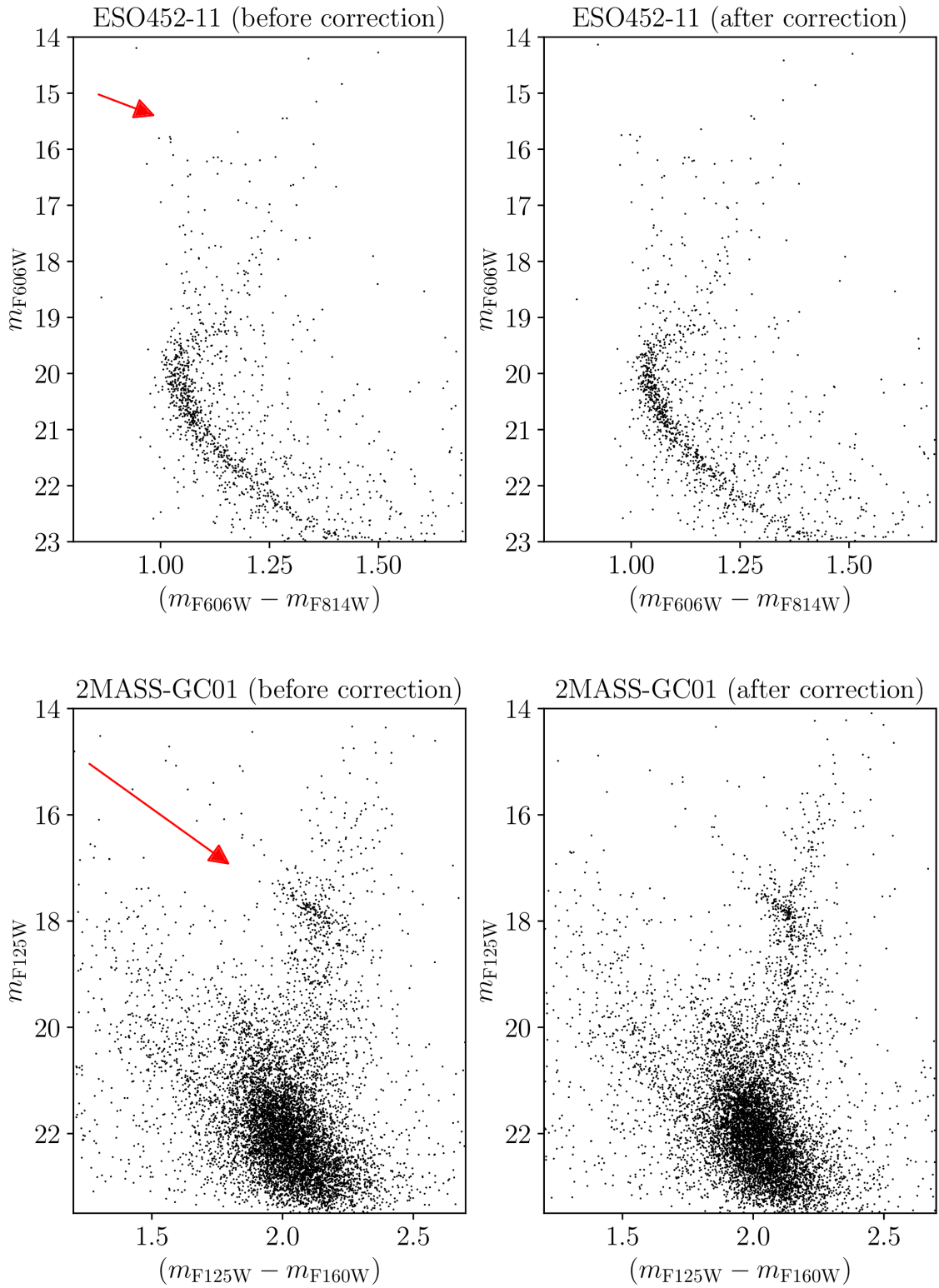


Fig. A.1: Comparison between the CMDs of ESO452-11 (upper row) and 2MASS-GC01 (lower row), before (left-hand panels) and after (right-hand panels) applying our differential-reddening correction. The red arrows represent the reddening vector obtained using the $E(B - V)$ values from the literature (Sect. 3.2), the A_λ assuming the Cardelli et al. (1989) law, and $R_V = 3.1$. The size of the arrows is reduced by a factor of three for clarity.